

TECHNICAL PAPER

Validation and automatic detection of the dispersive transport of the submarine outfall of Mar del Plata, Argentina

FEDERICO I. ISLA^{1,2,*}, LUIS C. CORTIZO^{1,2}, EDUARDO L. BLOTTA^{3,†}, JUAN I. PASTORE³, VIRGINIA L. BALLARIN³ and GRACIELA V. CUELLO^{1,2}

¹Instituto de Geología de Costas y del Cuaternario (IGCC), Universidad Nacional de Mar del Plata (UNMDP), Comisión de Investigaciones Científicas (CIC), Funes 3350, B7602AYL - Mar del Plata, Argentina. ²Instituto de Investigaciones Marinas y Costeras (IIMyC), Universidad Nacional de Mar del Plata (UNMDP), Consejo Nacional de Investigaciones Científicas y Técnicas (CONICET), Mar del Plata, Argentina. ³Instituto de Investigaciones Científicas y Tecnológicas en Electrónica (ICYTE), Universidad Nacional de Mar del Plata (UNMDP), Consejo Nacional de Investigaciones Científicas y Técnicas (CONICET), Mar del Plata, Argentina.

ORCID *Federico I. Isla*  <https://orcid.org/0000-0002-4930-0907>, *Eduardo L. Blotta*  <https://orcid.org/0000-0002-0256-3064>, *Virginia L. Ballarin*  <https://orcid.org/0000-0002-5648-6463>, *Graciela V. Cuello*  <https://orcid.org/0000-0001-6977-9962>



ABSTRACT. The submarine outfall of Mar del Plata city at Camet was projected considering the mean and maximum of forecasted sewage discharges, the inner-shelf depth, coliform concentration and its decay (T90) mainly induced by sunlight effect and costal salinity. In 2016 the outfall was operating with a length of 3,810 m and diffusers in the last 526 m. An economical method to monitor its performance in relation to the surroundings, is remote-sensing techniques, applying either visible or radar images. Tidal currents parallel to the coast are responsible for the transport of the sedimentary plume in the far field, after a primary dilution from a depth of 11 m. Visible images (1.5 to 6 m spatial resolution) are effective in monitoring the plume entrained in the upper portion of the water column. These analyses led to study the interaction between waves and coastal currents. Radar images (30 m resolution X and C bands) permit to survey the slick-alike plume that differs from the environment water by the surface roughness. Comparing both techniques visible images can distinguish the different colours of the plume; instead, the radar images are showing the surface roughness from the slick-alike plume. The main advantage of active sensors is that they can map the plume during a cloudy weather and even during night time.



*Correspondence:
fisla@mdp.edu.ar

†Deceased 14 October 2023

Received: 18 September 2023
Accepted: 13 December 2023

ISSN 2683-7595 (print)
ISSN 2683-7951 (online)

<https://ojs.inidep.edu.ar>

Journal of the Instituto Nacional de
Investigación y Desarrollo Pesquero
(INIDEP)



This work is licensed under a Creative
Commons Attribution-
NonCommercial-ShareAlike 4.0
International License

Key words: Sewage plume, coastal monitoring, radar images, Mar del Plata, Argentina.

Validación y detección automática del transporte dispersivo del emisario submarino de Mar del Plata, Argentina

RESUMEN. El emisario submarino de Mar del Plata en Camet fue proyectado considerando las descargas cloacales promedio y máximas previstas, la profundidad de la plataforma vecina, la concentración de coliformes y el decaimiento (T90) inducido por la luz solar y la salinidad. En 2016 el emisario operaba con una longitud de 3.810 m con difusores en los últimos 526 m. Un método poco oneroso para analizar su comportamiento en relación a su entorno es la aplicación de técnicas de teledetección tanto en el espectro visible como mediante imágenes de radar. Las corrientes de marea paralelas a la costa son responsables de una pluma sedimentaria en el campo lejano, luego de una dilución primaria desde una profundidad de 11 m. Las imágenes visibles (resolución espacial de 1,5 a 6 m) son efectivas para monitorear la pluma extendida en la capa superior del mar. Estos análisis permiten el estudio de la interacción entre olas y corrientes costeras. Las imágenes de radar (resolución de 30 m en las bandas X y C) permiten relevar plumas superficiales semejantes a derrames

de aceites por su rugosidad. Comparando ambas técnicas las imágenes visibles pueden distinguir plumas de diferentes colores del agua; por el contrario, las imágenes de radar están mostrando diferencias en la tensión superficial. La principal ventaja de los sensores activos es que permiten monitorear la pluma durante tiempo nuboso incluso sin luz solar.

Palabras clave: Pluma cloacal, monitoreo costero, imágenes de radar, Mar del Plata, Argentina.

INTRODUCTION

Water quality is crucial for the success of bathing areas. Many touristic cities have failed to improve sewage systems or combined sewage networks and therefore are subject to special concern, some of them with irreversible consequences. Several engineering and management options can be implemented: pollution prevention, pre-treatment and recycle-reuse (National Research Council 1993). Monitoring requires also dynamic modelling analyses of the municipal storm-water effluents (Moffa 1996). On the other hand, coastal structures (groin fields or pluvial networks) can reduce the water quality in bathing areas (Isla et al. 1998; Morea 2011).

Active sensors have been largely applied to monitor oil slicks and those comprised as 'slick alike' (Gade and Alpers 1999; Brekke and Solberg 2005; Hang and Duong 2009; Marghany and Hashim 2012; Marghany 2014). Oil reduces the Bragg scattering and therefore these areas look dark, although they can be subject to errors since they can be confused with organic films, grease ice, wind front areas, sectors sheltered by rocky outcrops, rain cells, internal waves or upwelling zones (Ferraro et al. 2010). The performances of sewage outfalls by radar (SAR) images have been applied in different coasts (Axiak et al. 2000; Di Giacomo et al. 2004).

In a previous contribution, the simulation of the projected submarine outfall of Mar del Plata at Parque Camet (Figure 1) was performed in order to forecast the behaviour of the future pipeline located on the inner shelf (Isla and Casanelli 2000). According to these authors, two different models were applied:

- A) The primary dilution considered the merging of the sewage at the ocean surface (Updated Muellenhoff model; Muellenhoff et al. 1985).
- B) At the far-field scale, tidal currents were taken as the main process affecting the future plume (AQUASEA program; Vatnaskill 1992).

That simulation was based on several premises:

1. The operation depth of the outfall was about 11 m;
2. the length of the outfall was originally projected as 3 km;
3. coastal tidal currents reversed parallel at the nearshore;
4. the outfall discharge could vary between 3.5 and 8.6 m³ sec⁻¹ (mean discharge 4.8 m³ sec⁻¹);
5. sewage total coliform concentrations vary between 10⁷ to 10⁹ coliforms in 100 ml;
6. the total coliform concentration at the coast was known as very low (16 to 70 coliforms in 100 ml);
7. the T90 (time for the decayment of 90% of the coliform bacteria) was estimated to vary between 1.2 h (sunny day, high-energy wave conditions) to 10 h (cloudy day, low-energy conditions).

In the present contribution, remote-sensing techniques were applied in order to map the behaviour of Mar del Plata sewage outfall in operation since 2016 (Scagliola et al. 2021). Different plumes surveyed were analysed in response to the inner-shelf dynamics, and compared to the simulations performed in 1999 (Isla and Casanelli 2000). The performance of this sewage disposal is crucial for touristic purposes in terms of the bathing quality of the northern beaches of the city (Figure 1).

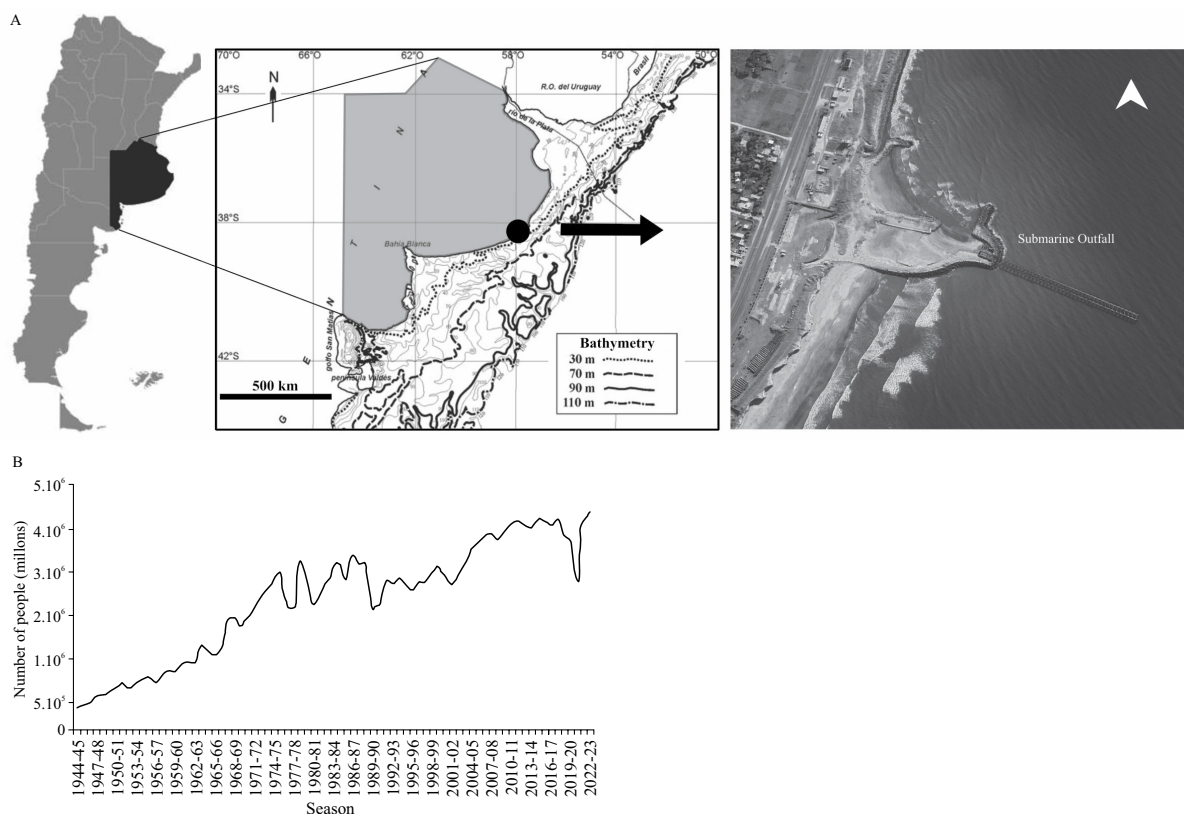


Figure 1. A) Location map indicating Mar del Plata city and the submarine outfall. B) Estimated number of tourists arriving to Mar del Plata city during summer between 1944 and 2023 (data provided by the Tourism Office of Mar del Plata City Hall).

Mar del Plata city and Camet outfall

The inner shelf close to Camet ($37^{\circ} 55' 30''$ S- $57^{\circ} 31' 40''$ W), 3 km north of Mar del Plata, was object of several oceanographic and substrate analyses (Isla and Aliotta 1999; Isla and Casanelli 2000; Elías et al. 2004, 2005). This coast has a micro tidal regime with breaker wave heights of less than 1.3 m (Isla et al. 2018). According to nautical charts of the Hydrographic Survey (SHN) currents are bidirectional and parallel to the contour depths. These wave altitudes can increase significantly during extratropical storms arriving from the southeast, locally called *sudestada*. However, Mar del Plata has a bimodal wave approach dominated by waves coming from the SE, and from the ENE (Isla 2010, 2014). Coastal currents are dominated

by tidal effects with mean velocities of 0.15 m s^{-1} and maximum of 0.45 m s^{-1} according to three current meters located at about 10 m (Isla and Aliotta 1999; Isla and Casanelli 2000; Isla 2014). Bathymetric changes were reported for 1967, 1970 and 1996 (Isla and Aliotta 1999) while the most recent detailed bathymetry was performed in 1998 (Isla and Casanelli 2000).

The area affected by the sewage disposal was colonised by mussels and polychaetes that take advantage of the organic-rich sewage (Jaubet et al. 2013). The outfall finally constructed in 2014 is 3,810 m long, with 3,284 m of polyethylene pipeline of 2 m diameter plus 526 m of the extreme interval with diffusers. This extreme has 130 elevated tubes of 150 mm diameter every 4 m. The pipeline is therefore composed of 315 tubes of 12 m each.

MATERIALS AND METHODS

In order to validate the simulations of the plume performed in 1999 (Isla and Casanelli 2000), remote sensing techniques were applied. Water density differences between the sewage outfall and the environment were already simulated applying the physical models RSB and UM to calculate the primary dilution at the surface (Muellenhoff et al. 1985; Roberts et al. 1989). Coastal currents were measured at different depths and different tidal conditions (Isla et al. 1998); three current meters provided data during one month (Isla and Aliotta 1999; Isla and Casanelli 2000). Visible images were selected with minimum cloud coverages. High-resolution Spot images (1.5 m resolution in panchromatic, 6 m in multispectral) were analysed (8 from 2016 and 4 from 2017). At the same time, SAR (Synthetic aperture radar) images were also tested to analyse plume extensions during cloudy or night conditions. These pansharpened products had been previously corrected with a geographic projection WGS84. Band X, Cosmo Skymed images (12 scenes) were analysed to map plume extensions. Mode Scansar and the product type GEC-B (with geographic coordinates) were analysed with a spatial resolution of 30 m and swath coverage of 100 km. Polarisation method was V-V, descending from N to S, with an incidence angle of 40°. Sentinel 1.B (band C) images (12 scenes) were handled with an IWS polarization VV (Table 1). Pre-processing consisted of calibration to convert the digital numbers (DN) to backscatter coefficient (σ^0), and reduction of the speckle noise with filters 3×3 and 5×5 , both using the Lee and Refined Lee procedures. These images were also projected to coordinates UTM-WGS84.

An expert system within a Google Earth Engine platform (GEE) was developed in order to lead to the automatic detection of plumes reducing the complexity of handling geospatial data. Algorithms were stated using JavaScript or Python routines.

The first step was to define the geometry of the plume (polygon) limited by geographic coordinates (Figure 2). Subsequently, the plume was defined according to date, VV polarisation, and the resulting geometry spatially delimited in the SAR image.

Once the search area was defined in space and time, the segmentation procedure of Otsu adaptive threshold is operated (Otsu 1979; Mehmet and Bulent 2004). The original speckle noise was eliminated, preserving the original shapes, using morphological openings and closing in the reconstructions (Serra 1982, 1988). Several morphologic parameters can be extracted, such as area, perimeter, as well as shorter and longer axes:

1. Area (A): spatial extension of the object in m^2 .
2. Perimeter (P): length (m) of the border of the object.
3. Complexity (C): takes a small numerical value for regions with simple geometry and a large one for complex geometrical regions (Del Frate et al. 2000; Topouzelis 2007). It is defined as:

$$C = \frac{P}{2\sqrt{\pi A}}$$

4. Shape factor (SP): describes the general shape of the object (Keramitsoglou 2005).
5. Major axis length: length (in pixels) of the major axis of the ellipse that has the same normalized second central moments as the region.
6. Minor axis length: length (in pixels) of the minor axis of the ellipse that has the same normalized second central moments as the region.

RESULTS

Passive sensors

From the analysis of the Spot images, it was possible to discriminate moments when the plume was subject exclusively to primary dilution; i.e. the

Table 1. Characteristics of the SAR images processed.

Satellite temporal	Mode	Swath (km)	Ground resolution (m)	Incidence angle	Polarization	Temporal resolution
Cosmo-Skymed Band(X)	Scansar Wide-Region	100	30 × 30	20°-60°	Single HH o HV VH oVV	< 12 h
Sentinel-1 Band (C)	Interferometric Wide Swath	250	5 × 20	20°-45°	Dual VV-VH HH-HV	12 d

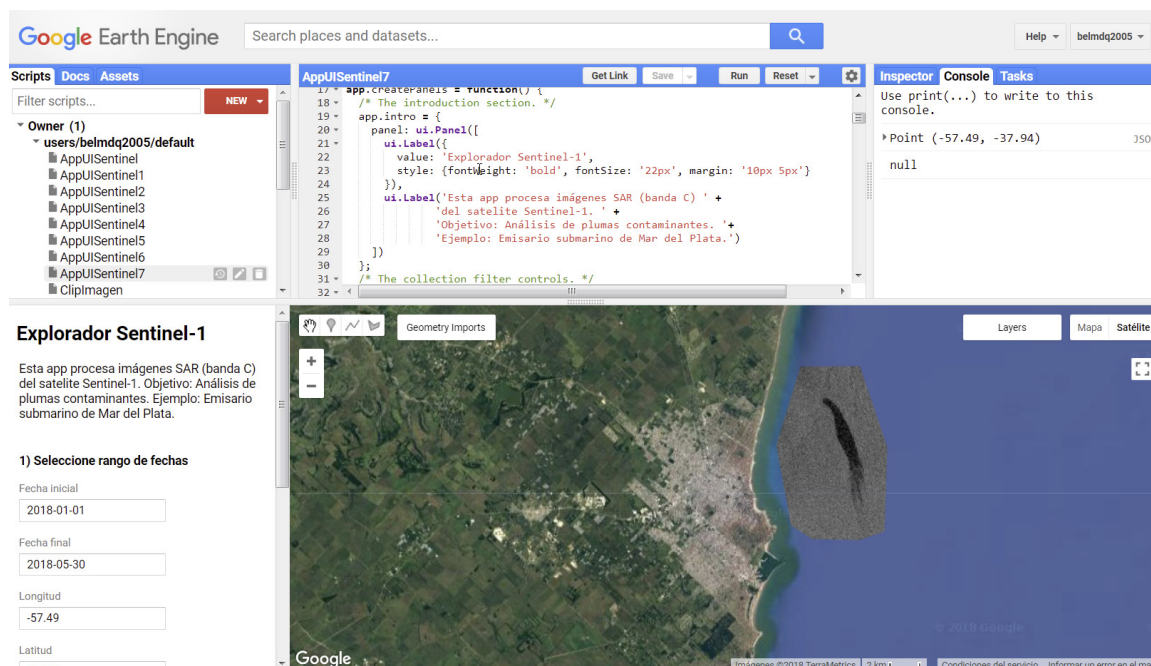


Figure 2. Interface Google Earth Engine from a SAR image (Sentinel-1, Band C; January 1, 2018).

plume was limited to the top of the diffusers (Figure 3 A). These situations occurred when there was no wind and the tide is at slack water during low or high tide. When tidal currents were at maximum velocity, and with high concentration of discharge, the plume had a maximum extension parallel to the isobaths. Although similar conditions were simulated in 1999, the plume has a narrowness that was

assigned to wave effects. As previously mentioned, waves in Mar del Plata have a bimodal frequency: six small waves with periods of about 10 s are forward by three waves of higher altitude (Isla 2010). This wave climate is caused by the interaction of sets coming from the ENE (lower waves) and from the SE (higher waves). It is assumed that the time recurrence of these higher waves conditions the

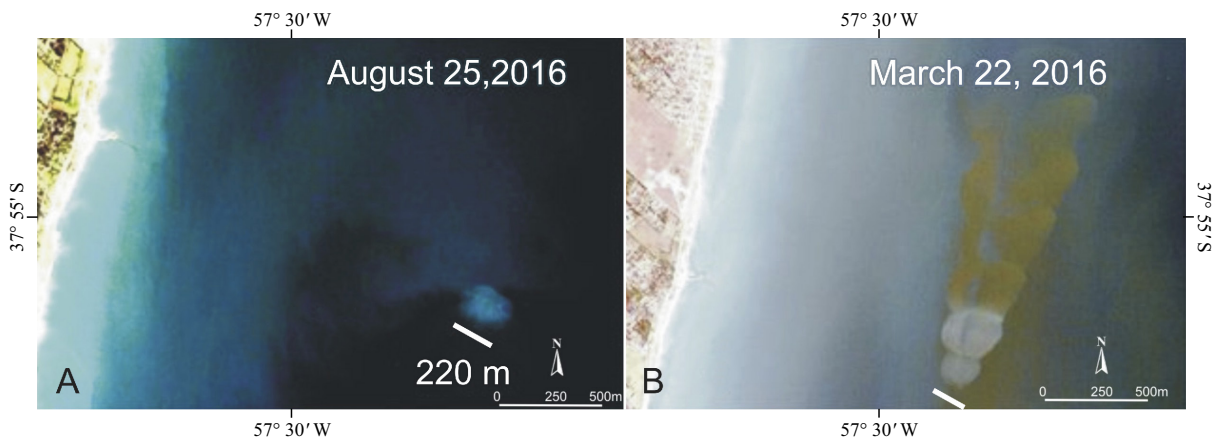


Figure 3. Comparing SPOT images it is possible to monitor the coastal dynamics interacting with the plume. A) Primary dilution stage. B) Maximum current stage.

width of the plume (Figure 3 B). In fact, the behaviour of the plume at the inner shelf could not be related to meteorological data collected at the Mar Plata airport at Camet, as this station has urban-canopy effects (Isla and Perez 1998).

On the other hand, it can be noted that the width of the plume depends on the volume of sediment discharging and the instantaneous velocity of the tidal current. The effects of the maximum waves cause significant variations of the width of the plume (Figure 4). Unfortunately, there were no simultaneous measurements of the wave and wind conditions during the capture of each scene.

Active sensors

Radar images have the capability of recognising slicks through differences detected in the surface roughness between them and the surrounding ocean water (Figure 5). At the same time, radar images can operate during night and even with a cloudy cover (Nunziata and Migliaccio 2015).

Automatic detection

The processes based on the GEE allowed to detect automatically different behaviours of the sewage plume of Mar del Plata city (Figure 6).

Plumes shapes responded mainly to the velocity of tidal currents. Tidal currents were measured with three current meters located precisely and at depths of 10-12 m (Isla and Aliotta 1999). With this information the surface transport in the far field was simulated (Isla and Casanelli 2000) and confirmed by both visible and radar images. Major and minor axes of these plumes differ according to tidal excursion (Isla et al. 1998) and water and concentration discharges (Table 2), as assumed in the simulations performed (Isla and Casanelli 2000).

DISCUSSION

The behaviour of outfall plumes is a key issue when sewage systems are operating in terms of coastal water quality (Di Giacomo et al. 2004; Ji et al. 2012; Roth et al. 2016; Alfredini et al. 2017). In Southeastern Australia, three outfalls have improved the bathing quality of 31 beaches. However, the water quality diminishes after rainfalls due to the bacteria transported by stormwater pipelines to those beaches (Manning et al. 2019).

Passive sensors permit to discriminate plumes and oil slicks when they are contrasting from clear seawater (Klemas 2013). Floating litter can also be

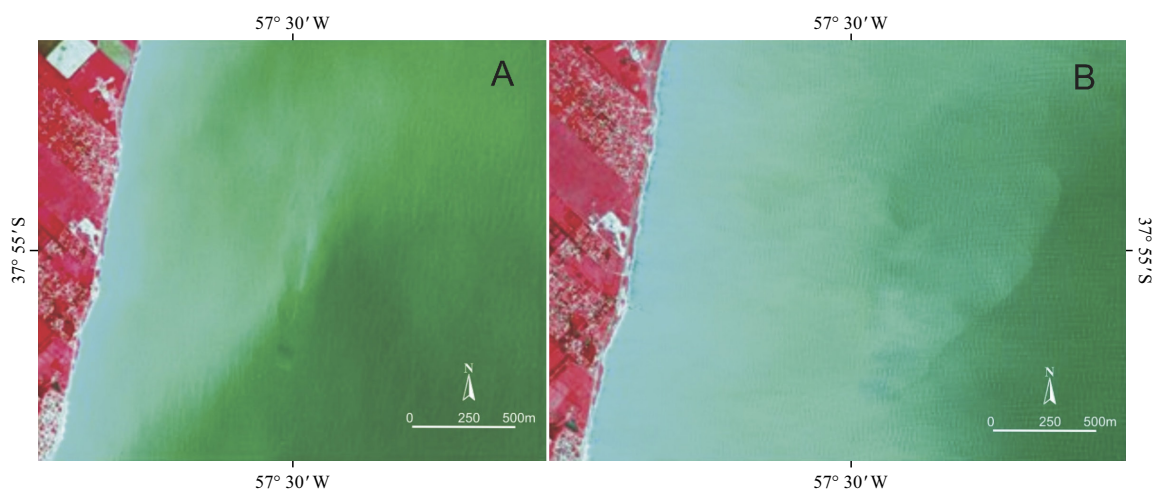


Figure 4. The interaction between tidal currents and wave-wind action is responsible for the widths of the plume applying SPOT images (false colour composition). Plume behaves narrowly during maximum currents (November 4, 2016; less wave effects and significant current velocity to the north) and widens when waves and wind induce more dispersion (November 10, 2016; less current velocity to the north and more dispersion induced by wave effects).

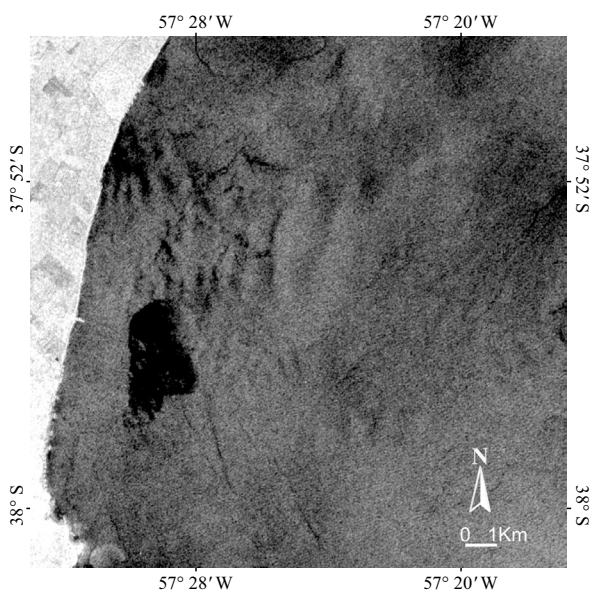


Figure 5. Cosmo Skymed image, band X (April 22, 2016) enhances the differences in the surface roughness between clear water and the plume composed of detergents (slick-alike plume).

monitored with remote sensing techniques (Hafeez et al. 2018). Multiple sensing techniques are recommended to monitor spills (Leifer et al. 2012).

Some spills do not last much on surface water. For example, oil spills from the Gulf of Mexico, together with wind velocities over 7 m s^{-1} can make slicks smaller as the oil is dispersed and mixed. In this sense, during strong currents and low-energy winds slicks can extend more than 20 km lasting more than 48 h (Daneshgar Asl et al. 2017).

The widths of the plume were assigned to the velocity of the tidal current and concentrations of the effluent. The narrowness of the plume was attributed to the interactions of different wave approaches. The sewage outfall of Camet can be masked in the visible spectra with turbidity spots produced by the suspended matter derived from the action of waves on the silty-loess substrate, outcropping as submerged patches and abrasion platforms. In that sense, active sensors do not include these colour-effects errors.

In sum, both remote-sensing techniques, passive and active, can be applied to monitor oil slicks. Visible images monitor the sedimentary plume in relation to the penetration depth in the ocean water and plume's turbidity (Figure 7). Radar images recognise plumes in the surface, differencing the roughness between clear (oceanic) water and the

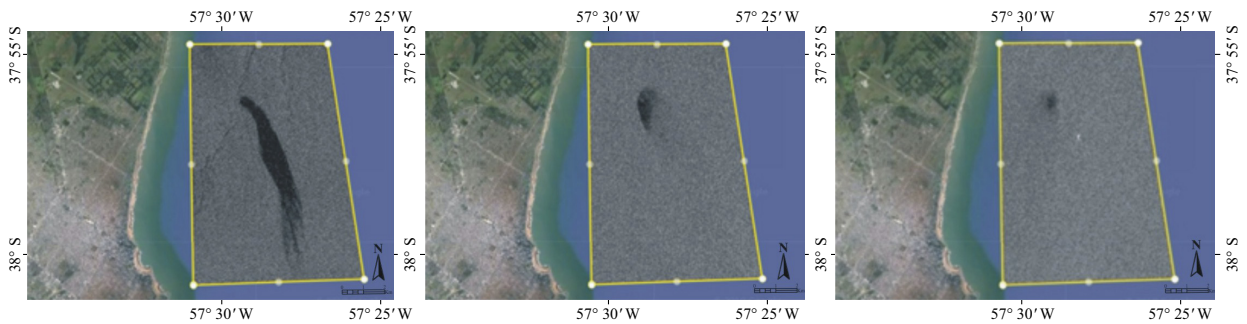


Figure 6. SAR image of Mar del Plata city outfall plumes at different conditions. From left to right: January 1, 2018 (tidal currents from north to south), January 23, 2018 (slight current towards the north), and February 16, 2018 (without currents).

Table 2. Images processed and shape parameters of the sewage outfall of Camet.

Image	Area (m ²)	Perimeter (m)	Minor axis (m)	Major axis (m)	Width REC (m)	Length REC (m)	Area rectangle (m ²)	Complexity	Shape factor
Img20180216	161,600	5,133	438	585	600	680	408,000	3.6027	0.75
Img20180123	744,300	12,526	637	1,761	770	1,900	1,463,000	4.096	0.36
Img20180111	4,748,700	44,504	1,086	6,883	2,870	6,940	19,917,800	5.761	0.16

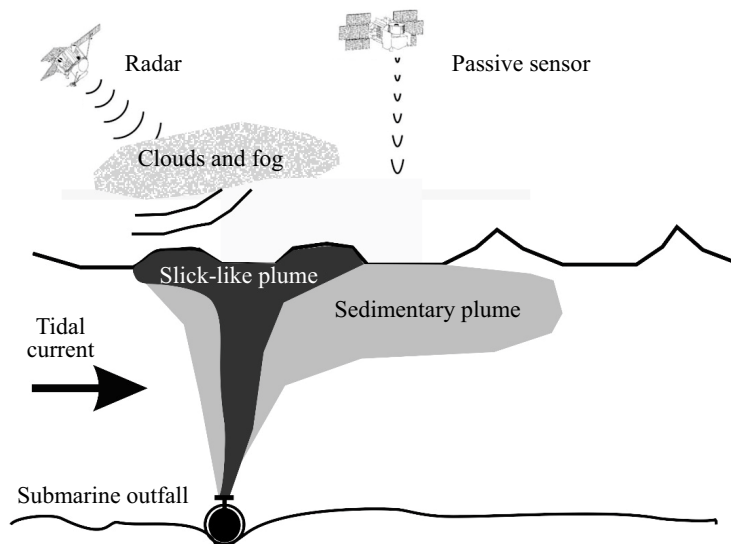


Figure 7. Schematic diagram showing the performance of passive and active sensors in relation to the sewage plumes. Passive sensors distinguish different colours of the turbidity plume in relation to the sea water. Active sensors detect differences in the roughness of the water surface induced by the viscosity of the slick-alike plume.

slick-alike surfactants (mostly detergents). Similar differences were observed in the application of optical (MODIS) and radar (Envisat ASAR) images for mapping pollution was concluded in San Pedro Bay, Los Angeles (Holt et al. 2017).

CONCLUSIONS

1. Spot images confirm assumptions of previous papers in the sense that tidal currents are the main processes involved in the behaviour of the plume of the submarine outfall of Camet.
2. Images enable the discernment of situations dominated by primary dilution (slack water and without wind), as well as those dominated by maximum velocity of the tidal currents. Differences in the wave climate affect the surface distribution of the plume in a higher way than local winds.
3. Optical images can distinguish the plumes due to colour contrasts between different conditions of surface turbidity.
4. Radar images distinguish plumes by differences in the surface roughness in relation to that of the ocean.

ACKNOWLEDGEMENTS

Financial support was provided by the Argentina National Space Activities Commission (CONAE) ‘Anuncio de oportunidad orientado a las Ciencias del Mar’. Marcelo Scagliola (Obras Sanitarias Mar del Plata) provided information about the operation of the sewage treatment plant. Two anonymous reviewers helped to improve the manuscript.

Author contributions

Federico I. Isla: conceptualization, investigation,

methodology, supervision, validation, visualization, writing-review and editing. Luis C. Cortizo: investigation, methodology, software, validation, visualization. Eduardo L. Blotta: methods, Earth Engine processing. Luis I. Pastore: Google Earth Engine processing. Virginia L. Ballarin: methods, image processing. Graciela V. Cuello: bottom sampling, validation.

REFERENCES

- AGENZIA SPAZIALE ITALIANA. 2007. COSMO-SkyMed System Description & User Guide. Roma: ASI (Agenzia Spaziale Italiana).
- ALFREDINI P, ARASAKI E, DE MELO BERNARDINO JC. 2017. Santos sea outfall wastewater dispersion process: physical modelling evaluation. *J Coast Res.* 33 (1): 173-190.
- AXIAK V, PAVLAKIS P, SIEBER AJ, TARCHI D. 2000. Re-assessing the extent of impact of Malta’s (Central Mediterranean) major sewage outfall using ERS SAR. *Mar Pollut Bull.* 40 (9): 734-738.
- BREKKE C, SOLBERG AHS. 2005. Oil spill detection by satellite remote sensing. *Remote Sens Environ.* 95: 1-13.
- DANESHGAR ASL S, DUKHOVSKOY DS, BOURASSA M, MACDONALD IR. 2017. Hindcast modeling of oil slick persistence from natural seeps. *Remote Sens Environ.* 189: 96-107.
- DEL FRATE F, PETROCCHI A, LICHTENEGGER J, CALABRESI G. 2000. Neural networks for oil spill detection using ERS-SAR data. *IEEE Trans Geosci Remote Sens.* 38 (5): 2282-2287.
- DI GIACOMO PM, WASHBURN L, HOLT B, JONES BH. 2004. Coastal pollution hazards in southern California observed by SAR imagery: stormwater plumes, wastewater plumes, and natural hydrocarbon seeps. *Mar Pollut Bull.* 49: 1013-1024.
- ELÍAS R, VALLARINO E, SCAGLIOLA ME, ISLA F. 2004. Pre impact macrobenthos conditions at a sewage disposal site: inner shelf of Mar del

- Plata (38° S-57° W, SW Atlantic). *J Coast Res.* 20 (4): 1176-1182.
- ELÍAS R, PALACIOS JR, RIVERO MS, VALLARINO EA. 2005. Short-term responses to sewage discharge and storms of subtidal sand-bottom macrozoobenthic assemblages off Mar del Plata City, Argentina (SW Atlantic). *J Sea Res.* 53: 231-242.
- FERRARO G, BASCHEK B, DE MONTPELLIER G, NJOTEN O, PERKOVIC M, VESPE M. 2010. On the SAR derived alert in the detection of oil spills according to the analysis of the EGEMP. *Mar Pollut Bull.* 60: 91-102.
- GADE M, ALPERS W. 1999. Using ERS-2 SAR images for routine observation of marine pollution in European coastal waters. *Sci Total Environ.* 237/238: 441-448.
- HAFEEZ S, WONG MS, ABBAS S, KWOK CYT, NICHOL J, LEE KH, TANG D, PUN L. 2018. Detection and monitoring of marine pollution using remote sensing technologies. In: FOUZIA HB, editor. *Monitoring of Marine Pollution*. IntechOpen. DOI: <https://doi.org/10.5772/intechopen.81657>
- HANG LM, DUONG ND. 2009. Oil spill detection and classification by ALOS PALSAR at Vietnam East Sea. 7th FIG Regional Conference Spatial Data Serving People: Land Governance and the Environment. Building the Capacity. p. 1-12.
- HOLT B, TRINH R, GIERACH MM. 2017. Stormwater runoff plumes in the Southern California Bight: a comparison study with SAR and MODIS imagery. *Mar Pollut Bull.* 118: 141-154.
- ISLA FI. 2010. Natural and artificial reefs at Mar del Plata, Argentina. *J Integr Coast Zone Manage.* 10 (1): 81-93. DOI: <https://doi.org/10.5894/rgci175>
- ISLA FI. 2014. Variaciones espaciales y temporales de la deriva litoral, SE de la Provincia de Buenos Aires, Argentina. *Rev Geogr Sur.* 5 (8): 24-41.
- ISLA FI, ALIOTTA S. 1999. Storm dispersal of volcanogenic sands from Buenos Aires: where heavy-metal concentrations are heavy-mineral segregations. *Mar Georesources Geotechnol.* 17 (4): 357-370.
- ISLA FI, CASANELLI A. 2000. Simulación del transporte dispersivo con decaimiento: futuro emisario submarino de Mar del Plata. *Revista de la Asociación Argentina de Sedimentología.* 6 (1-2): 61-73.
- ISLA FI, CORTIZOLC, MERLOTTO A, BERTOLA G, PONTRELLI ALBISETTI M, FINOCCHIETTI C. 2018. Erosion in Buenos Aires province: coastal-management policy revisited. *Ocean Coast Manage.* 156: 107-116.
- ISLA FI, PEREZ C. 1998. Efectos de la capa urbano-canópea en los registros meteorológicos de Camet, Mar del Plata. 5° Jornadas Geológicas y Geofísicas Bonaerenses, CIC, Mar del Plata. 2. 59-60.
- ISLA FI, PEREZ GUZZI J, ZAMORA A, FOLABELLA A. 1998. Aportes de coliformes a la costa de Mar del Plata por vías naturales e inducidas. *Revista Thalassas.* 14: 63-70.
- JAUBET ML, GARRAFO GV, SÁNCHEZ MA, ELÍAS R. 2013. Reef-forming polychaetes outcompetes ecosystem engineering mussels. *Mar Pollut Bull.* 71: 216-221.
- Ji H, PAN S, HAN X. 2012. Effect of wastewater discharge on Jiangsu coastal environment, China. *J Coast Res.* 65 (1): 54-59.
- KERAMITSOGLU I. 2005. Automatic identification of oil spills on satellite images. *Environ Modell Software.* 21: 640-652.
- KLEMAS V. 2013. Airborne remote sensing of coastal features and processes: an overview. *J Coast Res.* 29 (2): 239-255.
- LEIFER I, LEHR WJ, SIMECEK-BEATTY D, BRADLEY E, CLARK R, DENNISON P, HU Y, MATHESON S, JONES CE, HOLT B, et al. 2012. State of the art satellite and airborne marine oil spill remote sensing: application to the BP Deepwater Horizon oil spill. *Remote Sens Environ.* 124: 185-209.
- MANNING SS, DIXON JP, BIRCH GF, BESLEY CH. 2019. Deepwater ocean outfalls: a sustainable solution for sewage discharge formega-coastal cities (Sydney, Australia): influences on beach

- water quality. *Mar Pollut Bull.* 145: 691-706
- MARGHANY M. 2014. Oil spill pollution automatic detection from MultiSAR satellite data using genetic algorithm. In: MARGHANY M, editor. *Advanced Geoscience Remote Sensing*. In-techOpen. Chapter 3. p. 51-71. DOI: <https://doi.org/10.5772/58572>
- MARGHANY M, HASHIM M. 2012. Automatic detection algorithms for oil spill from Multisar data. Kuala Lumpur: *Progress in Electromagnetics Research Symposium Proceeding*. p. 1796-1800.
- MEHMET S, BULENT S. 2004. Survey over image thresholding techniques and quantitative performance evaluation. *J Electron Imaging*. 13: 146-165.
- MOFFA PE. 1996. The control and treatment of industrial and municipal stormwater. Van Nostrand Reinhold. 310 p.
- MOREA JP. 2011. Evaluación de impactos derivados de la construcción de una escollera en la intersección de las avenidas Constitución y Félix U. Camet. Mar del Plata, Argentina. *Revista de Estudios Marítimos y Sociales*. 4 (4): 175-184.
- MUELLENHOFF WP, SOLDATE AM JR, BAUMGARTNER DJ, SCHULDT MD, DAVIS LR, FRICK WE. 1985. Initial mixing characteristics of municipal ocean outfall discharges. Vol 1. *Procedures and Applications*. EPA/600/3-85/073a.
- NATIONAL RESEARCH COUNCIL. 1993. Managing wastewater in coastal urban areas. National Academy of Sciences. 477 p.
- NUNZIATA F, MIGLIOCCIO M. 2015. Oil spill monitoring and damage assessment via PolSAR measurements. *Aquat Procedia*. 3: 95-102.
- OTSU N. 1979. A threshold selection method from gray-level histogram. *IEEE Trans Syst Man Cybern.* 9 (1): 62-66.
- ROBERTS PJW, SNYDER WJ, BAUMGARTNER DJ. 1989. Ocean outfalls I: submerged wastefield formation. *J Hydraul Eng.* 115 (1): 1-25.
- ROTH F, LESSA GC, WILD C, KIKUCHI RKP, NAUMANN MS. 2016. Impacts of a high-discharge submarine sewage outfall on water quality in the coastal zone of Salvador (Bahia, Brazil). *Mar Pollut Bull.* 106: 43-48.
- SCAGLIOLA M, COMINO AP, ROBERTS P, BOTELHO D. 2021. The history of the Mar del Plata outfall system: a tale worth telling. *Hydrolink*. 6 p.
- SERRA J. 1982. *Image analysis and mathematical morphology*. Vol. 1. London: Academic Press.
- SERRA J. 1988. *Image analysis and mathematical morphology*. Vol. 2. London: Academic Press.
- TOPOUZELIS K. 2007. Detection and discrimination between oil spills and look-alike phenomena Through neural networks. *ISPRS J Photogramm Remote Sens.* 62 (4): 264-270.
- VATNASKILL. 1992. AQUASEA program. Reykjavik: Vatnaskill Consultant Engineers.

